CATALYSIS

Spin-mediated promotion of Co catalysts for ammonia synthesis

Ke Zhang†, Ang Cao†, Lau Halkier Wandall, Jerome Vernieres, Jakob Kibsgaard, Jens K. Nørskov*, Ib Chorkendorff*

Over the past two decades, there has been growing interest in developing catalysts to enable Haber-Bosch ammonia synthesis under milder conditions than currently pertain. Rational catalyst design requires theoretical guidance and clear mechanistic understanding. Recently, a spin-mediated promotion mechanism was proposed to activate traditionally unreactive magnetic materials such as cobalt (Co) for ammonia synthesis by introducing hetero metal atoms bound to the active site of the catalyst surface. We combined theory and experiment to validate this promotion mechanism on a lanthanum (La)/Co system. By conducting model catalyst studies on Co single crystals and mass-selected Co nanoparticles at ambient pressure, we identified the active site for ammonia synthesis as the B_5 site of Co steps with La adsorption. The turnover frequency of 0.47 ± 0.03 per second achieved on the La/Co system at 350°C and 1 bar surpasses those of other model catalysts tested under identical conditions.

Despite more than a century of application at massive scales, chemical synthesis of ammonia remains a subject of highly active current research. Ammonia is not only the basis for fertilizer production but also a prospective energy carrier or storage intermediate in sustainable energy systems (*1*–*3*). Currently, ammonia is primarily produced by means of the Haber-Bosch process, in which nitrogen (N_2) and hydrogen (H_2) react over a promoted iron (Fe) catalyst at quite harsh reaction conditions (150 to 200 bar, 400° to 500°C). Large-scale, centralized facilities are required for the Haber-Bosch process, mainly because capital investment increases exponentially with pressure (*4*). To enhance compatibility with small-scale green hydrogen production facilities, operation under lower pressures would be beneficial. Decreasing the pressure, however, requires lowering the temperature, or else the process is limited by the gas-phase equilibrium. Consequently, there has been a search for a more efficient catalyst that can operate at lower temperatures and hence lower pressure (*5*–*15*). Alternatives to the Fe-based catalysts include rubidium (Ru), cobalt (Co), and nickel (Ni) promoted by additives or supports consisting of metal hydrides (*5*, *6*), amides (*7*), and electrides (*8*).

To explain how Co and Ni, which are very poor in pure form at activating N_2, can become active when combined with promoters such as lithiuim (Li) (*16*), barium (Ba) (*10*), and calcium (Ca) (*10*, *14*), our groups proposed a spin-mediated promotion mechanism for these magnetic materials (*17*). Extensive density functional theory (DFT) calculations and analysis suggested that when adsorbed promotors quench the magnetic moment of the adjacent Co or Ni atoms on the surface, these atoms can then bind N_2 in the dissociative transition-state geometry more strongly, hence promoting the N_2 activation process. Of the promoters that theory suggests can most effectively quench the surface Co magnetic moment, while still being at least partially reducible, lanthanum (La) stands out (*17*).

We have shown experimentally that La-promoted Co steps are indeed very active for ammonia synthesis as predicted by theory, by using Co single crystals and mass-selected Co nanoparticles (NPs) as two well-defined model systems. By evaporating La onto the flat Co(0001) and stepped $Co(10\bar{1}15)$ single crystals and comparing the respective activities, we identified La-promoted Co steps as the active site. The observed turnover frequency (TOF) of 0.47 ± 0.03 s^{-1} on $La/Co(10\bar{1}15)$ is more than two times greater at 350°C and 1 bar than those of the potassium (K)–promoted Fe(111) or Fe step sites that are believed to be the active sites in the current commercial ammonia catalysts (*18*–*21*). In addition, we have demonstrated the La promotion effect on mass-selected Co NPs supported on a partially reducible La precursor (such as LaN), allowing La to migrate to and activate the Co surface. By varying the Co particle size systematically, we provide strong combined experimental and theoretical evidence that the activity is linearly related to the number of similar type of step sites found on the $Co(10\bar{1}15)$ surface.

Previous works by Ye *et al.* have shown LaN-supported Co (Co/LaN) to be quite efficient for ammonia synthesis (*11*–*13*). Bolstered by DFT calculations, they proposed a dual active site contributing to the high activity, where the nitrogen vacancies generated in the metal nitride are responsible for the activation of N_2, and the Co is mainly responsible for H_2 activation. We disagree with this interpretation and show that the active site is a Co step promoted by La. By identifying the active site, we were able to quantify its extraordinary activity in comparison with the conventional catalyst, thus providing a guiding principle for scaling the active site to a real high-surface-area catalyst.

Theoretical investigation of the most active sites for La-promoted Co

La-promoted Co surfaces are predicted to be very active in N_2 bond scission owing to the spin-mediated promotion effect (*17*), which comes on top of the usual electrostatic promotion effect (*22*, *23*), as the result of the charge transfer from La to Co (supplementary materials). The decrease in the transition-state energy for N_2 dissociation on La-Co induced by the electrostatic effect and spin effect are −0.35 and −0.57 eV, respectively (*17*). The spin-mediated promotion relies on the combination of two effects: (i) Adsorption energies of both intermediates and the N-N transition state are more negative (stronger bond) on nonmagnetic than on magnetic surfaces, and (ii) many promotors quench the spin moment of the nearby Co or Ni atoms (Fig. 1A and figs. S1 to S2). The local nature of the spin quenching turns out to stabilize the transition state more than the N adsorption energy, opening the possibility of circumventing the traditional scaling relation between the two (Fig. 1B). For further explanation of this effect, we refer to (*17*), figure 3D, and the text therein. That is, N_2 activation is rendered more favorable without proportionally strong blocking of the surface by adsorbed N. Thus, Co promoted by La exhibits extraordinarily high activity that is clearly superior to that of the best-known K-Fe(111) and cesiuim (Cs)–promoted Ru catalysts, as illustrated in the calculated activity heatmap (Fig. 1B).

In the present work, we extended the work in (*17*) by systematically studying all the most likely exposed surface facets of Co in addition to $Co(10\bar{1}5)$ theoretically (fig. S3) to identify the most active surface site. We found that La plays a substantial role in decreasing the barrier for N_2 dissociation (rate-limiting step) on all Co surfaces (Fig. 1C and figs. S4 to S12). In particular, the stepped Co surfaces containing B_5 sites, such as Co(0001)-B and $Co(10\bar{1}5)$ (structures are shown in fig. S2), are most active; the terrace Co(0001) exhibits the least activity, even with La promotion. Like most adsorbates, including the N-N dissociation transition state, La tends to adsorb at the Co step sites instead of at terrace sites, according to the built surface-phase diagram (figs. S13 and S14), meaning that the most active Co B_5 site is also the most favorable adsorption site for La. More details and discussions are available in the supplementary materials.

Department of Physics, Technical University of Denmark, Kongens Lyngby, Denmark.
*Corresponding author. Email: jkno@dtu.dk (J.K.N.); ibchork@fysik.dtu.dk (I.C.)
†These authors contributed equally to this work.

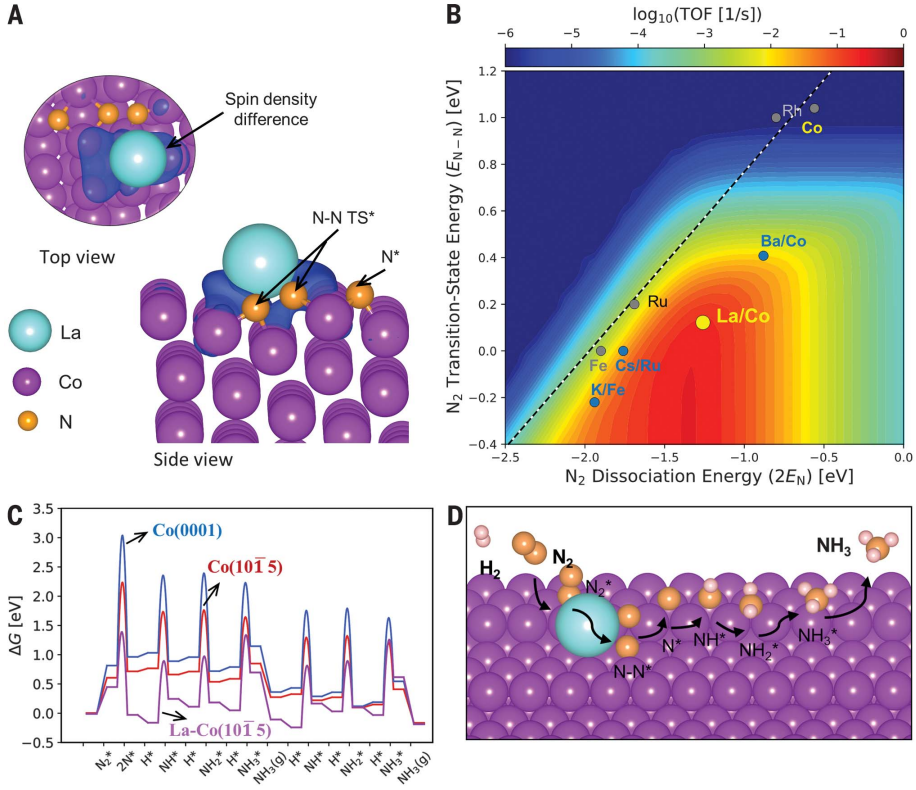

Fig. 1. Activity volcano for ammonia synthesis. (**A**) The spin density difference at the adsorption site of N* and N–N transition state on La promoted Co(10$\bar{1}$5), where the blue cloud indicates isosurfaces of spin density depletion. Purple, light blue, and orange spheres indicate Co, La, and N atoms, respectively. (**B**) 2D activity heatmap describing the theoretically calculated steady-state rate per site (TOF) for NH_3 synthesis as a function of N_2 transition-state energy (E_{N-N}) and N_2 dissociation energy ($2E_N$). Temperature (T) = 400°C, pressure (P) = 1 bar, H_2:N_2 = 3:1, and N_2 conversion = 0.01%. The dashed scaling line indicates the clean stepped transition-metal surfaces. (**C**) Calculated free energy diagram for ammonia synthesis on Co(0001), Co(10$\bar{1}$5), and La-Co(10$\bar{1}$15) under the same reaction conditions modeled in (A). (**D**) Reaction paths of ammonia synthesis on La-Co(10$\bar{1}$5), where purple, light blue, orange, and pink spheres indicate Co, La, N, and H, respectively.

On this basis, we conclude that the active stepped Co with La adsorption is also thermodynamically stable under reaction conditions. The favorable reaction pathway and optimized adsorption sites for key adsorbates on representative stepped Co(10$\bar{1}$5) is depicted in Fig. 1D for visualization. The above theoretical results therefore suggest that the predicted efficient La/Co(step) system should be fruitful for experimental testing.

Experimental verification on model catalyst of Co single crystals promoted by La

We performed model catalyst studies of ammonia synthesis at ambient pressure over two types of Co single crystals, a stepped Co(10$\bar{1}$15) and a terraced Co(0001), by evaporating La to achieve different coverages and comparing the activity. Herein, the step B_5-riched Co(10$\bar{1}$15) surface can be regarded as a 6.58° tilted vicinal surface of flat Co(0001), ideally with one single atomic step for every approximately eight terrace atoms (*24*). The deposition rate of La was calibrated by means of quartz crystal mass balance, and the coverage was double-checked with He^+ low-energy ion scattering (LEIS) by using the attenuation of the Co peak (983 eV) (fig. S22). The activity test was conducted in a newly designed ultrahigh-vacuum (UHV)–compatible high-pressure cell reactor (HPC), which can operate at 1 bar and up to 550°C (*25*). X-ray photoelectron spectroscopy (XPS) was performed before and after reaction (fig. S23), and no sign of La sintering or formation of hydride or nitride was observed.

As shown in Fig. 2A, the clean Co(10$\bar{1}$15) is inactive under the test conditions (1 bar, N_2+ $3H_2$, 350°C), whereas it is readily activated by evaporated La. The reaction rate versus La coverage on Co(10$\bar{1}$15) shows that the rate reaches maximum at ~0.15 monolayers (ML) and plateaus up to 0.5 ML. Further increasing La loading on the Co surface results in reduced activity. This volcano-shaped dependence of ammonia synthesis activity against La coverage can be explained as follows. At low La coverage (<0.15 ML), the evaporated La preferentially adsorbs to the most stable and relatively abundant B_5 sites, as demonstrated in figs. S6 and S7, thus accordingly inducing a linear relation between the total activity and the La coverage as expected. As the La coverage increases to 0.5 ML, La adsorbs on the less active Co sites such as the terrace, which contribute only marginally to the activity, resulting in a sluggish plateau region. Upon further increasing the La coverage, the activity drops off gradually because the Co active site is blocked by La and eventually completely disappears at full La coverage. Above all, on this volcano-like dependence curve of apparent activity on La coverage, activity on the left leg is limited by the La coverage, whereas that on the right leg is hampered by the insufficient number of Co B_5 sites. A medium coverage of La as a promotor on a rhodium (Rh) surface for an optimized performance toward hydrogen oxidation reaction was reported recently (*26*).

To reinforce the above conclusion that the activity is solely dominated by B_5 steps, as we previously observed for Ru (*27*), we used a flat Co(0001) to compare with the stepped Co(10$\bar{1}$15). Both pristine single crystals are inert. As shown in Fig. 2B, Co(0001) exhibited only a minute increase of activity upon deposition of 0.2 ML of La, which is significantly lower in comparison with that of Co(10$\bar{1}$15) with an equivalent La loading. We suggest that the small increase comes from the few steps that will always be present on a (0001) surface. This result directly supports the theoretical prediction that the enhanced catalytic activity is primarily attributed to the presence of La-promoted Co B_5 step sites.

Further verification on model catalyst of mass-selected Co NPs supported on LaN

After the success of the model catalyst study based on single crystals, we moved on to model catalyst studies with higher complexity that are more related to the real catalytic systems. To bridge this material complexity gap, we used monodispersed Co NPs of various sizes supported on reducible LaN as the second well-defined model system to execute cross validation for the theory prediction.

As demonstrated in Fig. 3A, by using a well-established UHV cluster source system (*28*, *29*), Co NPs of masses ranging from 4.4×10^4 to 1.4×10^6 amu (corresponding to sizes ranging from 2.5 to 8.0 nm) were selected out and deposited onto LaN thin films. The LaN substrate was prepared by means of reactive magnetron sputtering in a chamber connected to the UHV system. X-ray diffraction analysis

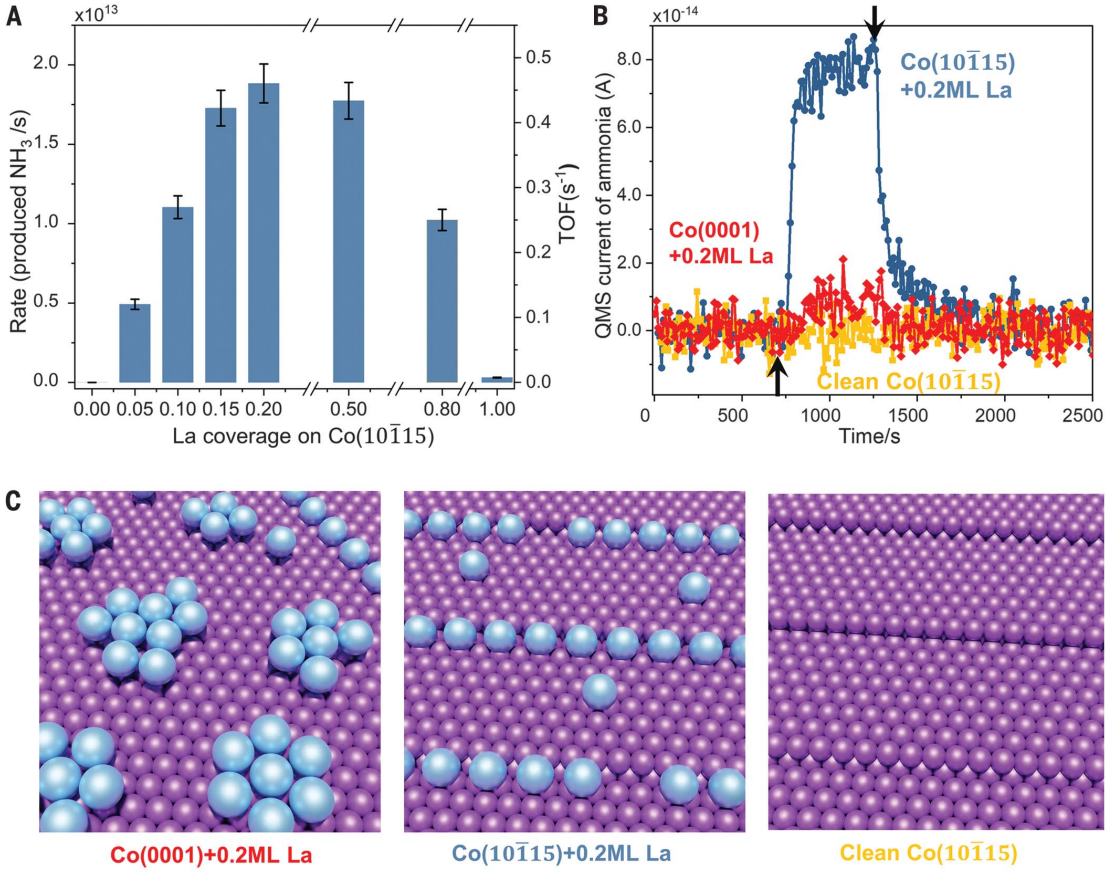

Fig. 2. Ammonia synthesis test of La-evaporated hcp-Co single crystals. (**A**) Apparent reaction rate and TOF as a function of the La coverage on Co(10$\bar{1}$15). The error bars indicate the SD of tests on three independent samples. (**B**) QMS signal profiles of ammonia (mass 17 amu) tested on clean Co(10$\bar{1}$15), 0.2ML La on Co(10$\bar{1}$15), and Co(0001) at 350°C and 1 bar N_2+3H_2. The arrows indicate the beginning and end of the reaction. (**C**) Schematics of surface atomic configurations for tested samples in (B). Purple, Co atoms; Light blue, La atoms.

(XRD) and XPS characterization identified the face-centered cubic (fcc) structure and chemical state of LaN (figs. S24 and S25) (*30*). To avoid particle overlap, the loading of the Co NPs was limited to 5% projected surface area coverage for NP sizes of 2.5 and 3 nm and 10% for NP sizes of 3.5 to 8 nm. After preparation, the sample was transferred in the UHV system and tested in the HPC, which features a sensitivity high enough to analyze the extremely low levels of ammonia formed on the Co particles of loadings of <100 ng (*25*).

Transmission electron microscopy (TEM) images and size distribution of the as-deposited three size ranges of Co NPs/LaN samples show homogeneous and clean Co NPs monodispersed on substrate, with well-defined size and loading (Fig. 3, B to E). The size distribution was measured from the TEM images as described in the supplementary materials. The average Co NP diameters of masses 7.6×10^4, 2.6×10^5, and 1.4×10^6 amu were measured as 3.6 ± 0.3, 5.0 ± 0.3, and 8.1 ± 0.2 nm, respectively. Compared with the respective calculated diameters of 3, 4.5, and 8 nm assuming a perfectly spherical particle with metal bulk density, the measured sizes are slightly larger, which is induced through rapid oxidation of Co NP surfaces to CoO and Co_3O_4 after exposure to air (*31*). To evaluate thermal stability of the Co NPs, fresh samples of the same masses were redeposited and treated in HPC under reaction conditions and then imaged with TEM. As shown in Fig. 3, F to I, the reaction conditions do not result in noticeable sintering or modification of size distribution. The excellent thermal stability renders the mass-selected Co NPs a well-defined model system to explore size-dependent properties in this study.

Ammonia synthesis activities of samples with 2.5- to 8.0-nm Co NPs supported on LaN are presented in Fig. 4A. The activity monotonically grows with decreasing particle size of the Co NPs over the investigated size range. All the apparent activities shown have been normalized to 10% projected coverage, so the size dependence indicates strong correlation between the density of active site and Co NP size. Furthermore, because Co NPs supported on C were inert under the conditions (350°C, 1 bar) (Fig. 4F), the presence of LaN for the activity is essential. We next addressed the nature of the active site of the LaN-supported Co NPs by means of DFT calculation, providing further experimental evidence to substantiate this understanding.

Extensive studies have revealed that Co NPs of sizes <20 nm possess fcc rather than the hexagonal close-packed (hcp) structure known from bulk Co at room temperature by means of scanning transmission electron microscopy (STEM) (*31*), reflection high-energy electron diffraction (RHEED) (*32*), ex situ XRD (*33*), and in situ XRD (*10*) under NH_3 synthesis conditions. Thus, we adopted fcc-structured Co NPs to explore the nature of the active site on LaN-supported Co NPs.

We first built a Wulff construction (Fig. 4B, inset) by calculating the surface energy of all the low-energy facets of fcc Co, determining the most likely exposed surfaces on the particles (*34*). We then calculated the dissociation energy of N_2 (rate-limiting step) on the above selected Co surfaces with and without La promotion (Fig. 4B) and found that Co(110), Co(111)-B, and Co(211) (structures are provided in figs. S15 to S17) show the relative lowest barrier. On the basis of the surface diagram (Fig. 4C), in contrast to Co(110), La preferentially adheres to Co(111)-B and Co(211) that possess B_5 sites. We further support the existence of La-Co(B_5) on the LaN-supported Co catalysts in light of the calculated phase diagram (Fig. 4C and fig. S18), which shows that La can be reduced out of LaN under the test conditions, owing to the strong bonding of the metallic La to the B_5 sites on Co. La/Co(B_5) is thus a good candidate for the active site

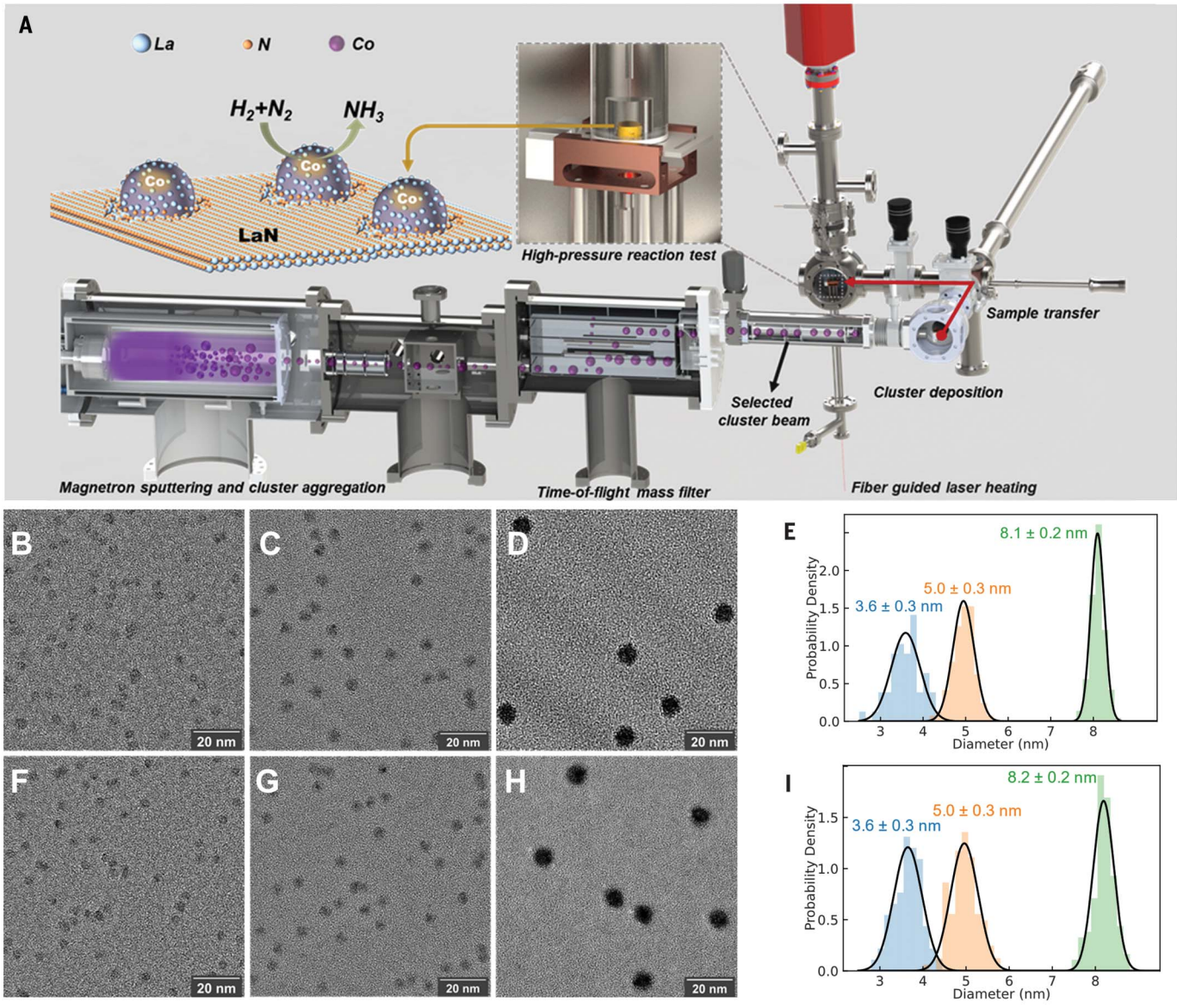

Fig. 3. Mass-selected Co NPs: Preparation, test, and stability. (**A**) Schematic illustration of the mass-selected NP deposition and test for ammonia synthesis at 1 bar in a UHV system. Reactive magnetron-sputtering deposited LaN thin film was used as the substrate. (**B** to **D** and **F** to **H**) Representative TEM images of three different masses of 4.3×10^4, 2.5×10^5, and 1.4×10^6 amu Co NPs on LaN [(B) to (D)] before and [(F) and (H)] after reaction conditions treatment at 350°C and 1 bar N_2+$3H_2$. (**E** and **I**) Corresponding size distributions (E) and (I) were determined by measuring the size in the TEM images (supplementary materials).

also on the LaN-supported Co NPs, same as the La-Co(10$\bar{1}$15) model catalyst.

We next investigated the relationship between the number of La/Co B_5 step sites and the measured catalytic activity. The active-site density is not directly given by the particle size distribution because only the steps containing B_5 sites are active for N_2 dissociation. To evaluate the fraction of B_5 sites on a Co particle, we built a basic particle shape of fcc-Co NPs using the calculated Wulff construction and then counted the number of Co atoms at the B_5 sites following the same manner as stated in previous work (*35*) (supplementary materials). Last, we derived the B_5 site volume density as a function of Co particle size (Fig. 4D).

A direct comparison of calculated volume density of B_5 sites and volume-averaged NH_3 productivity measured experimentally over differently sized Co NPs supported on LaN is shown in Fig. 4E, displaying an excellent linear correlation. Furthermore, if we use both values of the 2.5-nm Co NPs/LaN sample as a benchmark, the slope of the normalized fitted line between the two is 1 and roughly crosses the points (0, 0) and (1, 1) (fig. S19), which is even more explicit evidence that no activity is present beyond Co steps and that the TOF of La-Co(step) active site should be constant. We obtained similar results when hcp-structured Co NPs were assumed (fig. S20). By using the calculated number of B_5 atoms on each size of Co NPs, we were able to convert the measured rate of ammonia production to TOF per B_5 atoms. As shown in Fig. 4A, the TOF remains nearly constant at around 0.3 s^{-1} over the investigated size range, as expected.

TOF and activation energy of Co NPs/LaN and 20% La/Co(10$\bar{1}$15) measured at 1 bar and their comparison with various model catalysts are presented in Fig. 4F. Similar activation energies of 56 ± 2 kJ/mol and 54 ± 6 kJ/mol

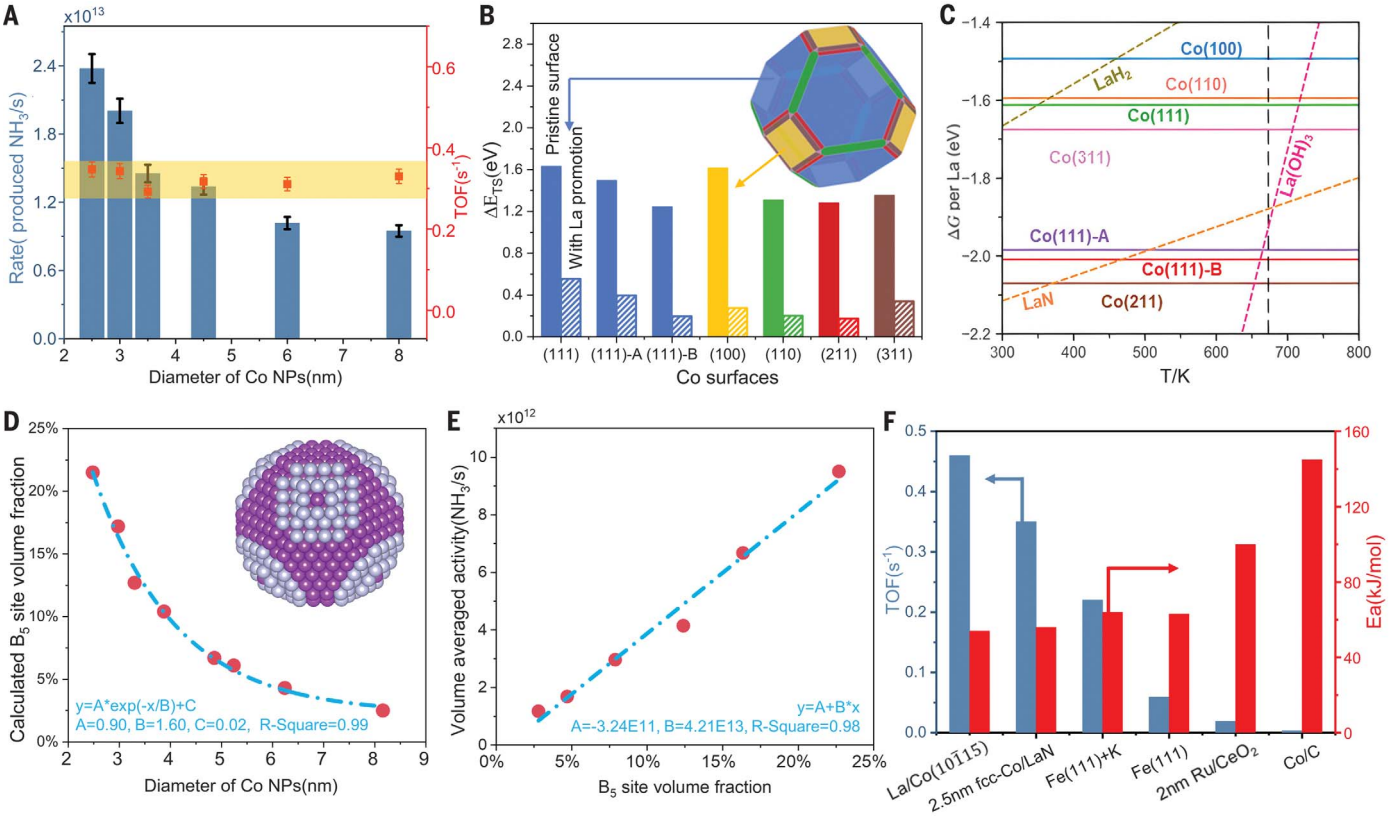

Fig. 4. Size dependence of ammonia synthesis on Co NPs/LaN and its correlation to DFT-calculated B_5 sites density on a fcc-Co surface. (**A**) Ammonia production rates of 2.5- to 8-nm-diameter Co NPs supported on LaN at 350°C and 1 bar N_2+3H_2. Projected Co coverages are 5% for 2.5- and 3-nm NPs and 10% for 3.5-, 4-, 6-, and 8-nm NPs. The apparent rates of 2.5- and 3-nm NPs were normalized to 10% coverage for comparison. TOF values were calculated on the basis of the number of B_5 sites on Co NPs of corresponding sizes calculated as shown in (D). The error bars of the apparent rate and TOF values indicate the SD of tests on three independent samples. (**B**) The calculated transition-state energies of different clean (solid bar) and La-promoted fcc-Co surfaces (hatched bar). (Inset) Wulff construction of fcc-Co particle with colored facets corresponding to the surfaces in bar chart. (**C**) The surface-phase diagram of La in different precursor compounds compared with La adsorbed on various Co surfaces under ammonia synthesis conditions [T = 673 K, P = 1 bar, H_2:N_2= 3:1, and $P(H_2O) = 10^{-7}$ bar]. Bulk species are shown as dashed lines, and metallic La adsorbed Co surfaces are shown as solid lines. Bulk energies are from experiments, except for LaN (supplementary materials). (**D**) The volume density of B_5 sites as a function of fcc-Co particle size, as calculated through analysis of the atomistic construction from Wulff structure in (B), inset. Atoms belonging to B_5 sites are shown in gray, and the rest are in purple. (**E**) Relations between the density of B_5 sites and volume averaged rate measured at 350°C, 1 bar. (**F**) TOF and activation energy overview on various model catalyst prepared and tested in our UHV system. Test conditions were 350°C, 1 bar, and 3H_2+N_2. The TOF of Fe(111) was calculated on the basis of the Fe atom density on top surface of 7.04×10^{14} cm^{-2}; 2 nm Ru/CeO_2 was calculated with respect to surface Ru atoms at the B_5 site of density described in (*35*). Activity of Co/C was not detected at 350°C; the TOF should be $<1 \times 10^{-3}$ s^{-1}, based on the estimated sensitivity limit of the HPC. The activation energy was calculated with rate measurements at 450° to 500°C and 1 bar.

of Co NPs/LaN and La/Co(10$\bar{1}$15) are in good agreement with the value of 64 kJ/mol (0.66 eV) calculated on the basis of the model of La/Co(10$\bar{1}$15) (fig. S12C), suggesting that both model catalyst systems share the same active site in nature as depicted in the DFT calculation. Comparable TOF values of La/Co(10$\bar{1}$15) and Co NPs/LaN further support this picture. Supreme intrinsic activity and low activation energy of the La/Co system among various model catalyst systems prepared and tested in our UHV system (Fig. 4F) signify major potential of the spin-mediated promotion mechanism in designing new catalysts for ammonia synthesis. Identification of the active site on the La/Co system paved the way for reaction mechanism illustration and further exploration into the dynamics of active site formation, which is important to improve the activity for practical application.

La-Co dynamics of Co NPs/LaN system during reaction

An essential stage to enable effective La promotion in Co NPs/LaN involves a redistribution of La from the LaN substrate to the Co NPs surface. To illustrate the composition evolution of the sample surface during the experiment, we performed XPS and He^+ LEIS characterization as snapshots after each experimental step in the process of LaN preparation, Co NP deposition, and ammonia synthesis testing in HPC. As seen in Fig. 5A, the LEIS spectrum of the as-prepared LaN film shows a La peak at 1073 eV, the intensity of which decreases after deposition of 10% 4.5-nm Co NPs on top, and correspondingly, Co shows a peak at 983 eV. They are easily resolved because of the sufficiently different atomic masses. The N peak is not visible in the spectrum because of the double matrix effect in LEIS on La-related surfaces (*36*). XPS confirmed the presence and stability of both La and N in their respective LaN valence states throughout the experiment (fig. S25).

After ammonia synthesis testing at 350°C in 1 bar H_2 and N_2, the LEIS spectrum showed higher intensity at the low-energy side, suggesting adsorption of H, N, and NH_x species on the surface, which may partially explain the drop of the Co peak and thus indicate the

reaction taking place on the Co surface. Co NPs were found to be rather stable against sintering under reaction conditions, as shown with TEM (Fig. 3, B to I) and XPS (fig. S25); thus, we can readily exclude a sintering-induced surface area decrease of Co during the reaction test. In contrast to Co, the intensity of the La peak after reaction increases nearly to the level of the pristine LaN film, which seems to hint toward the presence of La on top of the Co surface. This bears close resemblance to the well-known phenomenon of strong metal-support interaction (SMSI) (*37*, *38*)—that is, when a metal is supported on reducible oxide and subjected to high-temperature reducing conditions, it experiences partial decoration or even encapsulation by species migrating from the substrate. Because LaN exhibits reducibility in both calculations (Fig. 4C) and experiment (*11*, *12*), the inverse change in LEIS intensity of La and Co after the reaction appears to suggest a scenario illustrated in Fig. 5A, inset, which implies that during the test in an H_2 and N_2 environment at 350°C, La was reduced out and migrated onto the strongly adsorbed step sites of the Co surface, promoting on-site ammonia synthesis. The trend of sample self-activation was more obviously observed during a thermal cycling test of a freshly prepared sample of 4.5-nm Co NPs/LaN (fig. S26). The testing temperature began at 250°C, gradually increased to 350°C (upward tests), and then steadily decreased back to 250°C (downward tests), with a consistent interval of 25°C. Reaction rates obtained at the same temperature during downward tests were always higher than these obtained in the upward tests at 250° to 325°C and finally tested constant at 350°C, which indicates that the sample activation was complete at 350°C. Actually, high-temperature reduction induced activation of metal NPs supported on reducible rare-earth oxides for ammonia synthesis has been observed and attributed to SMSI. Reduced La and Ce species migrate from the La-Ce mixed-oxide substrate and then decorate the surface of supported Ru NPs to promote ammonia synthesis, although the promotion mechanism has different explanations (*39*–*41*).

Reduction of the substrate catalyzed by supported metal clusters in reductive conditions at high temperature has been reported previously (*42*, *43*). For the Co/LaN system subjected to ammonia synthesis conditions, we should also see the reduction of LaN as a precondition or in parallel to the migration of La species onto the Co surface. As observed in the SMSI, the species migrating from the substrate consistently take the form of an oxygen-deficient suboxide or, in some instances, have been reduced out to a metallic state (*44*). To provide further insight into the details of this process, we conducted isotope labeling experiments on samples with 4.5-nm Co NPs on LaN,

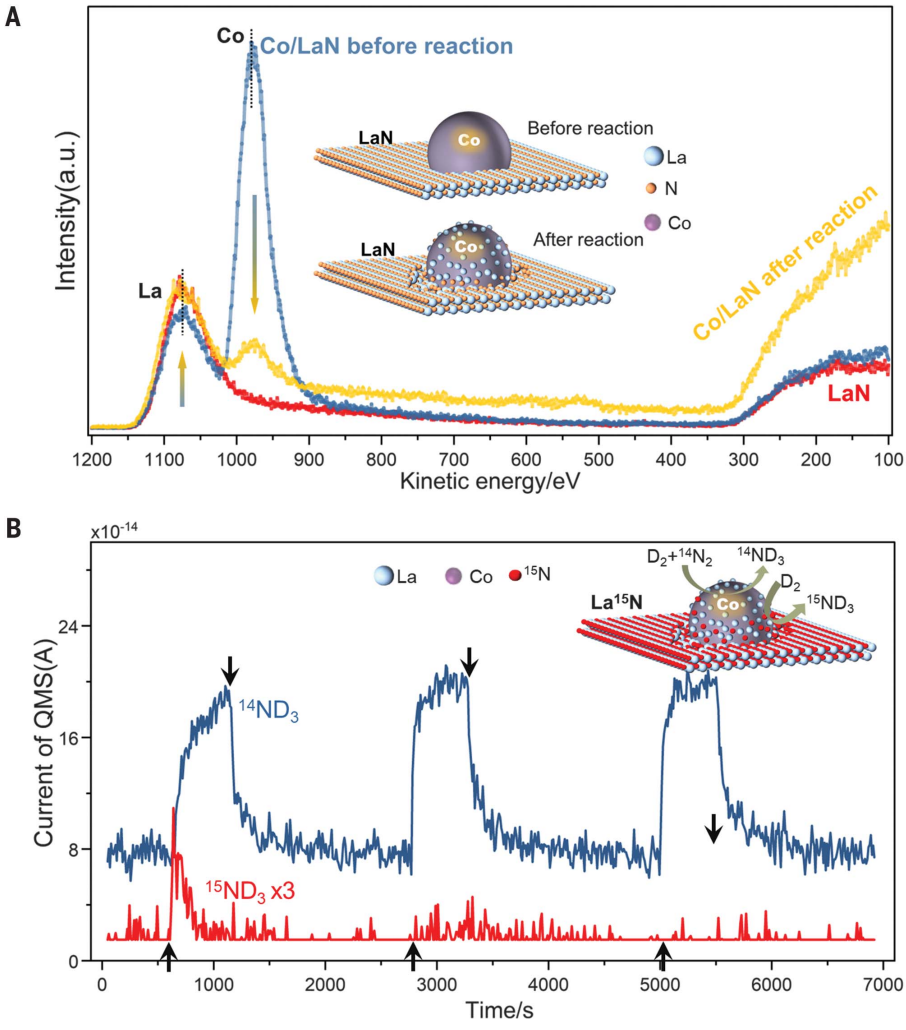

Fig. 5. La-Co dynamics in Co NPs/LaN system during test. (**A**) He^+ LEIS spectrum of as-prepared LaN, Co/LaN, and Co/LaN after test. He^+ energy is 1250 eV. (Inset) A schematic of La decoration on the Co NPs surface after reaction. (**B**) Isotopic labeling test of Co/La^{15}N in $^{14}N_2$+3D_2 for ammonia synthesis at 1 bar, 415°C. The signal of mass 21($^{15}ND_3$) is multiplied by 3. (Inset) A schematic of reduction of La$^{15}N_x$ species on the La surface or at the Co NPs/La^{15}N interface to produce the $^{15}ND_3$. Arrows indicate the beginning and end of the reaction.

as illustrated schematically in Fig. 5B, inset. Product from the reduction of LaN species, ammonia, is an indication of the activation process, and the number of ammonia molecules correlates with the La coverage on Co surface. To distinguish it from catalytically produced ammonia, we used a ^{15}N-labeled Co/La^{15}N sample for testing under an atmosphere of 1 bar $^{14}N_2$ and D_2. In this case, ammonia generated through the catalytic reaction should display a mass of 20 amu ($^{14}ND_3$) in quadrupole mass spectrometry (QMS), whereas ammonia resulting from the reduction of La$^{15}N_x$ should exclusively appear at a mass of 21 amu ($^{15}ND_3$).

A control experiment was conducted first with pristine La^{15}N to ensure that La^{15}N was not making ammonia under the test conditions. Subsequently, 15% 4.5-nm Co NPs was deposited on La^{15}N for the test. The QMS monitoring of signals at masses 20 and 21 amu during the three consecutive tests is presented in Fig. 5B. The results reveal a distinct and transient increase in the $^{15}ND_3$ signal at the onset of the first test, followed by a gradual decay to background levels over ~150 s. By contrast, production of $^{14}ND_3$ remains constant throughout the 500 s duration of the first test. $^{15}ND_3$ production can only be attributed to the reaction between D_2 and La^{15}N with the presence of Co NPs, and no other possible product should be observed at 21 amu. Transient appearance of $^{15}ND_3$ indicates the reduction of La$^{15}N_x$, and the migration of reduced La species toward the Co surface reached saturation during the first test. In the subsequent test, the $^{15}ND_3$ signal did not appear as before, whereas the $^{14}ND_3$ production not only persisted but also exhibited a higher initial rate, which indicates the completion of the activation process. This pattern of signal behavior remained consistent during

the third test, suggesting that the sample achieved a stable state after the first test. Assuming that each $^{15}ND_3$ molecule corresponds to one free La atom migrating to Co surface, the calculated number of La atoms from the transient $^{15}ND_3$ signal would result in a La coverage of ~0.50 ML or less on the Co surface, assuming all Co active sites are activated and no N isotope exchange occurs. Spontaneous redistribution of the reduced-out La on the Co surface was driven by the strong adsorption of La on Co steps, as indicated in Fig. 4C. Saturation coverage of La on the Co surface estimated should correspond to the surface fraction of the step site or slightly higher owing to the presence of other possible strong adsorption sites such as kicks on Co surface, which is consistent with the step density calculated in Fig. 4D. Furthermore, the La coverage estimated in the isotope experiment is generally consistent with the value on Co$(10\bar{1}15)$ to give rise to activity for ammonia synthesis shown in Fig. 2A.

Further active-site validation

The reaction mechanism of Co or Ni supported on reducible metal nitrides such as LaN or CeN has been previously proposed by Hosono's group to be a dual-site mechanism—that is, the nitrogen vacancies generated in the metal nitride are responsible for the activation of N_2, and the Co or Ni in this system is mainly responsible for H_2 activation. To examine this model, we introduced palladium (Pd) NPs supported on LaN because Pd is outstanding for H_2 dissociation and very poor for N_2 activation (*45*, *46*). As shown in fig. S27, 4.5-nm Pd NPs were deposited on a LaN surface, and the activity was compared with that of 4.5-nm Co NPs/LaN under identical test conditions. Absence of any discernible activity on Pd/LaN directly contradicts the dual-site mechanism. Instead, consistent theoretical and experimental evidence shown in this study identified the active site as La-promoted Co steps and validated a spin-mediated mechanism. We expect the application of the mechanism to guide the future design of new classes of catalyst based on accessible and more active materials such as promoted Co and Ni for ammonia synthesis under milder conditions.

REFERENCES AND NOTES

1. G. Ertl, *Angew. Chem. Int. Ed.* **47**, 3524–3535 (2008).
2. R. F. Service, *Science* **361**, 120–123 (2018).
3. C. H. Christensen, T. Johannessen, R. Z. Sørensen, J. K. Nørskov, *Catal. Today* **111**, 140–144 (2006).
4. D. E. Garrett, *Chemical Engineering Economics* (Springer Netherlands, 1989).
5. Y. Kobayashi *et al.*, *J. Am. Chem. Soc.* **139**, 18240–18246 (2017).
6. Q. Wang *et al.*, *Nat. Catal.* **4**, 959–967 (2021).
7. M. Kitano *et al.*, *Angew. Chem. Int. Ed.* **57**, 2648–2652 (2018).
8. M. Hara, M. Kitano, H. Hosono, *ACS Catal.* **7**, 2313–2324 (2017).
9. C. J. H. Jacobsen *et al.*, *J. Am. Chem. Soc.* **123**, 8404–8405 (2001).
10. S. Hagen *et al.*, *Chem. Commun.* **11**, 1206–1207 (2002).
11. T. N. Ye *et al.*, *Nature* **583**, 391–395 (2020).
12. T. N. Ye *et al.*, *J. Am. Chem. Soc.* **142**, 14374–14383 (2020).
13. T. N. Ye *et al.*, *J. Am. Chem. Soc.* **143**, 12857–12866 (2021).
14. Y. Inoue *et al.*, *ACS Catal.* **9**, 1670–1679 (2019).
15. V. Shadravan *et al.*, *Energy Environ. Sci.* **15**, 3310–3320 (2022).
16. P. Wang *et al.*, *Nat. Chem.* **9**, 64–70 (2017).
17. A. Cao *et al.*, *Nat. Commun.* **13**, 2382 (2022).
18. G. Ertl, M. Weiss, S. B. Lee, *Chem. Phys. Lett.* **60**, 391–394 (1979).
19. F. Bozso, G. Ertl, M. Weiss, *J. Catal.* **50**, 519–529 (1977).
20. G. A. Somorjai, N. Materer, *Top. Catal.* **1**, 215–231 (1994).
21. D. R. Strongin, G. A. Somorjai, *J. Catal.* **109**, 51–60 (1988).
22. J. J. Mortensen, B. Hammer, J. K. Nørskov, *Phys. Rev. Lett.* **80**, 4333–4336 (1998).
23. B. A. Rohr, A. R. Singh, J. K. Nørskov, *J. Catal.* **372**, 33–38 (2019).
24. K. M. Golder, J. Wintterlin, *ACS Catal.* **12**, 7199–7209 (2022).
25. K. Zhang, L. H. Wandall, J. Vernieres, J. Kibsgaard, I. Chorkendorff, *Rev. Sci. Instrum.* **94**, 114102 (2023).
26. M. Raab *et al.*, *Nat. Commun.* **14**, 7186 (2023).
27. S. Dahl *et al.*, *Phys. Rev. Lett.* **83**, 1814–1817 (1999).
28. Y.-R. Zheng *et al.*, *Nat. Energy* **7**, 55–64 (2022).
29. C. Roy *et al.*, *Nat. Catal.* **1**, 820–829 (2018).
30. B. Krause *et al.*, *J. Appl. Crystallogr.* **51**, 1013–1020 (2018).
31. J. Vijayakumar *et al.*, *Nat. Commun.* **14**, 174 (2023).
32. A. Kleibert *et al.*, *Phys. Rev. B* **95**, 195404 (2017).
33. M. Zybert *et al.*, *Catalysts* **12**, 1285 (2022).
34. B.-Y. Zhang, P.-P. Chen, J.-X. Liu, H.-Y. Su, W.-X. Li, *J. Phys. Chem. C Nanomater. Interfaces* **123**, 10956–10966 (2019).
35. K. Honkala *et al.*, *Science* **307**, 555–558 (2005).
36. A. A. Zameshin, A. E. Yakshin, J. M. Sturm, H. H. Brongerma, F. Bijkerk, *Appl. Surf. Sci.* **440**, 570–579 (2018).
37. F. Pesty, H.-P. Steinrück, T. E. Madey, *Surf. Sci.* **339**, 83–95 (1995).
38. M. G. Willinger *et al.*, *Angew. Chem. Int. Ed.* **53**, 5998–6001 (2014).
39. K. Sato *et al.*, *ACS Sustain. Chem.& Eng.* **8**, 2726–2734 (2020).
40. Y. Ogura *et al.*, *Chem. Sci.* **9**, 2230–2237 (2018).
41. Y. Ogura *et al.*, *ACS Sustain. Chem.& Eng.* **6**, 17258–17266 (2018).
42. R. Bliem *et al.*, *Angew. Chem. Int. Ed.* **54**, 13999–14002 (2015).
43. S. Kaiser *et al.*, *ACS Catal.* **11**, 9519–9529 (2021).
44. A. Beck *et al.*, *Nat. Commun.* **11**, 3220 (2020).
45. E. Skúlason *et al.*, *Phys. Chem. Chem. Phys.* **14**, 1235–1245 (2012).
46. M. Johansson *et al.*, *Surf. Sci.* **604**, 718–729 (2010).
47. K. Zhang, A. Cao, L. H. Wandall, J. Kibsgaard, J. K. Nørskov, I. Chorkendorff, Dataset for "Spin-mediated promotion of Co catalysts for ammonia synthesis". DTU Data (2023); https://doi.org/10.11583/DTU.24588576.v1.

ACKNOWLEDGMENTS

Funding: This project has received funding from Villum Fonden V-SUSTAIN (grant 9455) (K.Z., A.C., L.H.W., J.V., J.K., J.K.N., and I.C.) and the European Research Council (ERC) under the European Union's Horizon 2020 research and innovation program (grant 741860-CLUNATRA) (K.Z., A.C., J.V., J.K., and I.C.). **Author contributions:** Conceptualization: K.Z., A.C., I.C., and J.K.N. Data curation: K.Z., A.C., L.H.W., and J.V. Formal analysis: K.Z., A.C., and L.H.W. Investigation: K.Z. and A.C. Methodology – equipment design: K.Z. Visualization: K.Z., A.C., J.K., L.H.W., and J.V. Supervision: I.C., J.K.N., and J.K. Writing – original draft: K.Z., A.C. Writing – review and editing: K.Z., A.C., L.H.W., J.V., J.K., J.K.N, and I.C. **Competing interests:** The authors declare no competing interests. **Data and materials availability:** All data are archived at the Technical University of Denmark (DTU) (*47*). **License information:** Copyright © 2024 the authors, some rights reserved; exclusive licensee American Association for the Advancement of Science. No claim to original US government works. https://www.science.org/about/science-licenses-journal-article-reuse

SUPPLEMENTARY MATERIALS

science.org/doi/10.1126/science.adn0558
Materials and Methods
Supplementary Text
Figs. S1 to S27
Tables S1 to S4
References (*48*–*61*)

Submitted 20 November 2023; accepted 30 January 2024
10.1126/science.adn0558